**Atmospheric
Chemistry
and Physics
Discussions**

Influence of convection and aerosol pollution on ice cloud particle effective radius

J. H. Jiang[1], H. Su[1], C. Zhai[1], S. T. Massie[2], M. R. Schoeberl[3,*], P. R. Colarco[3], S. Platnick[3], Y. Gu[4], and K.-N. Liou[4]

[1]Jet propulsion Laboratory, California Institute of Technology, Pasadena, California, USA
[2]National Center for Atmospheric Research, Boulder, Colorado, USA
[3]NASA Goddard Space Flight Center, Greenbelt, Maryland, USA
[4]Department of Atmospheric Sciences, University of California, Los Angeles, USA

Correspondence to: J. H. Jiang (jonathan.h.jiang@jpl.nasa.gov)

ACPD

10, 23091–23108, 2010

Convection and aerosol pollution on ice cloud particle

J. H. Jiang et al.

Title Page

Abstract	Introduction
Conclusions	References
Tables	Figures

|◄ | ►|

◄ | ►

Back | Close

Full Screen / Esc

Printer-friendly Version

Interactive Discussion

Convection and aerosol pollution on ice cloud particle

J. H. Jiang et al.

Abstract

Satellite observations show that ice cloud effective radius (r_e) increases with ice water content (IWC) but decreases with aerosol optical thickness (AOT). Using least-squares fitting to the observed data, we obtain an analytical formula to describe the variations of r_e with IWC and AOT for several regions with distinct characteristics of r_e-IWC-AOT relationships. As IWC directly relates to convective strength and AOT represents aerosol loading, our empirical formula provides a means to quantify the relative roles of dynamics and aerosols in controlling r_e in different geographical regions, and to establish a framework for parameterization of aerosol effects on r_e in climate models.

1 Introduction

It is well known that aerosols can cause changes in cloud number concentration and therefore alter cloud particle size, which can result in changes of cloud lifetime, reflectance, and precipitation (e.g. Twomey, 1977; Albrecht, 1989; Lohmann and Feichter, 2005; Penner et al., 2006). To date, quantification of the indirect effects of aerosols on climate remains a challenging problem. One difficulty is to separate dynamic effects, for example, the convective updraft strength, from aerosol microphysical effects. Inadequate understanding of the relationship between microphysical and dynamical processes contributes to large uncertainties in model simulations of aerosol effects on clouds, precipitation and climate.

Recent studies (e.g. Jiang et al., 2008, 2009; Su et al., 2010) using collocated Aura satellite's Microwave Limb Sounder (MLS) and Aqua satellite's Moderate-resolution Imaging Spectroradiometer (MODIS) observations showed reduction of upper tropospheric (UT) ice cloud effective radius (r_e) in polluted clouds, defined by collocated carbon monoxide (CO) measurements higher than a certain threshold value. The enhanced CO values are positively correlated with aerosol optical thickness (AOT) for a number of geographical regions and seasons. Jiang et al. (2008, 2009) also showed

that r_e generally increases with convective intensity indicated by ice water content (IWC), as stronger convection produces more condensates and larger cloud particles. For different regions and seasons, the variations of r_e with IWC and CO (AOT) are different. Characterizing the regional differences of dynamic and aerosol effects quantitatively is needed for models to accurately simulate aerosol-cloud interactions.

Traditionally, the ice cloud particle size distribution is parameterized as a function of IWC following a gamma distribution (e.g. Matrosov et al., 1994; Evans and Stephens, 1995) or a bimodal distribution (e.g. Mitchell et al., 1996; Platt, 1997; Macfarqure and Heymsfield, 1997), neither of which takes into account the effect of aerosol on r_e (i.e. the first indirect effect of aerosols on clouds). In this paper, we use least squares fitting to the observations and derive an analytical formula to describe the r_e variations with convection and aerosol intensities in different geographical regions and seasons. This formula intends to provide a framework to quantify the relative effects of dynamics and aerosols on r_e, and to parameterize the first indirect effects of aerosols for use in climate models.

2 Data and approach

For this study, the MODIS r_e and AOT measurements are from Aqua MODIS MYD08-D3 and MYD04-L2 data sets, respectively (Platnick et al., 2003; Remer et al., 2005). The MLS IWC is from MLS Version 2.2 Level 2 data (Wu et al., 2009). The MODIS and MLS measurements are collocated by averaging the MODIS data onto the MLS footprints (Jiang et al., 2009). Although the MODIS AOT data are usually missing in the cloudy regions, the MODIS measurements have much higher horizontal resolution (~10 km×10 km) than the MLS measurements (~300 km along track and ~7 km cross track), thus the AOT data are available in about half of the data in which MLS detects cloud (i.e. when IWC>0).

The MODIS r_e measurement pertains to the top of cirrus clouds, with the vertical weighting function peaked at about 0.1 to 0.2 optical depth (~1–2 km depending on

cloud extinction) down from the cloud top (Platnick, 2000; Zhang et al., 2010). MLS detects ice clouds above 215 hPa, with IWC measurement vertically distributed at the pressure levels between 215 and 68 hPa, with a 3–4 km vertical resolution. Given that only the cloud top r_e is available from MODIS, we limit the analysis to those r_e measurements when IWC at 215 hPa is detectable by MLS, where clouds are likely associated with deep convection. We examine the cloud top r_e relationship as a function of the column aerosol loading (indicted by AOT) and convective strength (indicated by MLS IWC at 215 hPa) under the premise that the influence of lower level aerosols on clouds is propagated to deep convective cloud tops (e.g. Sherwood, 2002). For parameterization of r_e in climate models, it would be desirable to describe r_e as a function of aerosol concentration and cloud water content (CWC) at each vertical height. However, due to the limitation of the data, the current study aims to provide a heuristic framework for future height-resolved analysis. The bulk relationships obtained here are insightful for understanding of the dynamics and aerosol effects on convective cloud particle sizes.

We also use the outgoing longwave radiation (OLR) data from GEOS-5 (Goddard Earth Observation Systems, Version 5) analysis (Rienecker et al., 2008) to validate that MLS IWC at 215 hPa is a good index for convection. The GEOS-5 OLR data are also sampled onto the MLS foot-prints (Jiang et al., 2010).

For this study, the data from August 2004 to July 2008 are used.

3 Observed relationships

The relationship between MLS IWC measurements at 215 hPa and the GEOS-5 OLR for the tropical region (30° S to 30° N) is shown on Fig. 1. Consistent with previous studies (e.g. Su et al., 2006; Jiang et al., 2007, 2010), the 215 hPa IWC is shown to generally correlate well with the OLR (with correlation factor ≈ −0.3 for instantaneous measurements and ≈ −0.9 for annual gridded data) and thus can be used as an index for convective strength, approximately. We define the convective index (CONV) as

$$\mathrm{CONV}_i = \mathrm{IWC}_i / \overline{\mathrm{IWC}} \qquad\qquad (1)$$

where IWC_i represents each single MLS 215 hPa IWC measurement and $\overline{\mathrm{IWC}}$ is the mean of all the 215 hPa IWC samples.

Next, we examine the relationships among the MLS CONV index and MODIS measurements of ice cloud r_e and AOT from August 2004 to July 2008 between 50° S and 50° N. Figure 2a shows the MODIS r_e binned according to the CONV index. The thick black curve is the average r_e versus CONV curve that includes all values of AOT. It can be seen that when CONV is relatively small, r_e increases approximately linearly with IWC. When CONV is greater than ~1, the increase of r_e with CONV becomes slower or saturated as the maximum r_e may be limited by the settling velocities of the ice particles. The influence of aerosol on r_e is illustrated by grouping the r_e data for polluted clouds with AOT>0.4 (thin black curve) and for clean clouds having AOT<0.05 (blue curve). The r_e for the polluted clouds is about 2–4 μm smaller than the r_e for the clean clouds. Note that the clean cloud r_e increases faster with CONV than the polluted cloud r_e.

Figure 2b shows the relation of r_e to AOT. For 0<AOT<~0.1, r_e quickly increases with AOT. When AOT>0.1, r_e decreases at a rate of about 0.5 μm per 0.1 increase of AOT until AOT ~0.5, then the r_e decreasing rate becomes slower or stays approximately constant.

The dependence of r_e on CONV and AOT is further illustrated by the Bi-Variate Composite (BVC) plot of the r_e-CONV-AOT relation (Fig. 2c), in which the MODIS r_e data are binned according both to the MLS CONV and the MODIS AOT values. About 150 000 collocated MODIS and MLS measurements from August 2004 to July 2008 between 50° S to 50° N are used for the plot. The dotted lines show the occurrence frequency for each CONV-AOT pair. The BVC figure shows that r_e increases with CONV but decreases with AOT: the largest r_e resides where the convection (CONV) is largest and pollution (AOT) is lowest, i.e. strong convection in a clean environment. At constant CONV, the r_e decreases with increasing AOT, suggesting an influence of

aerosol loading on the cloud particle size. At constant AOT, r_e increases with CONV until CONV approaches $\sim$1. At the large CONV values (CONV$>\sim$1), r_e becomes approximately constant when AOT is $<\sim$0.3, but decreases with IWC in high polluted cases (AOT$>\sim$0.3).

4   Empirical fitting

In order to obtain a simple mathematical expression for the above observed r_e-CONV-AOT relation, we assume that the dependence of r_e on CONV and AOT is decoupled, i.e., $r_e = r_{aot} \cdot r_{conv}$, where r_{conv} denotes how cloud particle effective radius changes with CONV and r_{aot} represents the effect of aerosols on r_e. We write

$$r_{conv} = [1 - \exp(-\text{CONV}/\alpha)] \cdot \exp(-\beta\,\text{CONV}), \tag{2}$$

where α and β are the parameters that control how fast r_e changes with CONV. The reduction of r_e by aerosol effect is assumed to follow a power-law:

$$r_{aot} = \varepsilon \cdot \text{AOT}^{\eta}, \tag{3}$$

where η is a parameter that determines how strong the aerosol effect is, and ε is a scaling constant. A superposition of Eqs. (2) and (3) yields

$$r_e = \varepsilon \cdot \text{AOT}^{\eta} \cdot [1 - \exp(-\text{CONV}/\alpha)] \cdot \exp(-\beta\,\text{CONV}). \tag{4}$$

We then use least-squares fitting to the observed data with the empirical formula (4), i.e., to determine the parameters α, β, η, and ε, through minimizing the following cost function

$$\underset{\alpha,\beta,\eta,\varepsilon}{\text{cost}} = \sum_i \left[r_e^i - r_e(\text{CONV}^i, \text{AOT}^i, \alpha, \beta, \eta, \varepsilon) \right]^2 \tag{5}$$

where r_e^i (in µm) and AOT^i represent the ith sample of the observed r_e and AOT data, respectively, and CONV^i is computed from observed IWC (Eq. 1).

Convection and aerosol pollution on ice cloud particle

J. H. Jiang et al.

The least-square fittings are computed by using four years of MLS IWC and MODIS r_e and AOT measurements. The results of the fitted parameters for different regions are given in Table 1. Following the analyses by Jiang et al. (2009), the definitions for the different regions are: Global (LON: 0°–360°; LAT: 50° S–50° N); South America (LON: 270°–340°; LAT: 40° S–10° N); Southern Africa (LON: 0°–55°; LAT: 35° S–0°); Northern Africa (LON: –10°–45°; LAT: 0° S–25° N); South Asia (LON: 70°–120°; LAT: 10° S–15° N); and East Asia (LON: 90°–180°; LAT: 20°–45° N).

Substituting the fitted parameters into Eq. (4), we obtain r_e (μm) as functions of CONV and AOT for all of the above mentioned geographical regions. These empirical model results are plotted in Fig. 3 along with the observations. The χ^2/DOF (degrees of freedom) listed in Table 1 illustrates the convergence of the fitting for different regions. The closer is the value of (χ^2/DOF) to 1 (or less), the better is the fitting. We found that although all fittings converge after ~20 iterations, the best fittings are those for the Global, South America, Southern and Northern African regions. The empirical models for South and East Asia do not fit with the observations as well as the other four regions. The regional differences are discussed below.

5 Analyses of regional characteristics

5.1 Qualitative differences: the BVC plots

We display r_e as a function of CONV and AOT in Fig. 3 for a number of regions using both observations and the empirical fittings. Comparing with the observations (Fig. 3 left-column), the empirical models (Fig. 3 right-column) approximately capture the broad features of observed r_e-CONV-AOT relationships. For example, r_e, in general, increases with CONV but decreases with AOT, so that the largest r_e occurs when convection (CONV) is strong and pollution (AOT) is low.

At the global scale (Fig. 3a and b), increasing aerosol pollution tends to reduce cloud particle size, while increasing convection tends to enlarge cloud particle size. Strong

convection, however, also increases the distributions of aerosols into the UT. Thus, for the same columnar AOT, the UT ice clouds may be more affected by aerosols in regions of stronger CONV, indicated by a steeper gradient of r_e with increasing AOT, than in regions of weaker CONV.

For South America (Fig. 3c and d), the observed r_e increases with increasing convective strength, but varies less monotonically with AOT than in the global case. Large r_e is broadly distributed in low AOT regions, but the largest r_e is not collocated with the cleanest air. One reason may be that cloud particle size can increase with AOT in regions where moisture is abundant and cloud particles continue growing with increasing number concentration of cloud condensation nuclei (e.g. Ackerman et al., 2004). However, such a non-monotonic behavior is not captured by the empirical fitting, because the AOT dependence is chosen to be a monotonically decreasing function. In regions where CONV is larger than 1, the observed increase of r_e with CONV is not as sharp as in the global case, while the empirical model appears to produce larger r_e than the observation.

Southern Africa (Fig. 3e, f) and Northern Africa (Fig. 3g, h) regions are very similar to each other in that the maximum r_e is much smaller than the global case, resulting in weak r_e gradients for all values of CONV and AOT. It appears that r_e decreases with AOT more rapidly in Southern Africa than in Northern Africa.

South Asia (Fig. 3i, j) is very different from the rest of the geographical regions. The reduction of r_e with AOT is more pronounced both at the low ($<\sim0.8$) and high ($>\sim2$) ends of the CONV values. In the medium CONV values between 0.8 and 2, the reduction of r_e with AOT is slower than in the low and high CONV ranges, resulting in ice clouds having large ($>27\,\mu m$) r_e, extending into the high AOT (>0.4) range. This dependence of aerosol effects on convective regimes may indicate complicated coupling between aerosol forcing and meteorological conditions.

East Asia (Fig. 3k, l) has very irregular r_e changes with CONV and AOT. First, it seems to share a similar feature to South Asia in the medium CONV range, where the reduction of r_e with AOT is slow. Second, r_e is observed to rapidly increase with AOT

Title Page

Abstract | Introduction

Conclusions | References

Tables | Figures

◄ | ►

◄ | ►

Back | Close

Full Screen / Esc

Printer-friendly Version

Interactive Discussion

in regions where AOT is less than ~0.2 to 0.3 (Fig. 3k). This may be an indication of the influence of anthropogenic (e.g. incomplete combustion generated black carbon) aerosols that are very absorptive. The heat released by such aerosols might invigorate convection and thus increase cloud particle size (Menon et al., 2002). The first feature is simulated by the empirical model (Fig. 3l), while the second feature is not captured, which is the main reason for the large χ^2/DOF value and poor fitting in this region.

5.2   Quantitative differences: each term in the empirical model

The empirical model has several different terms (see Eq. 4). The first term, $[1 - \exp(-CONV/\alpha)]$, represents the growth of r_e with respect to CONV (Fig. 4a): when there is no convection (CONV→0), this term approaches 0. As CONV increases, it grows quickly. For CONV>1, it approaches the maximum of 1. This increasing effect of convection on r_e is the strongest in Northern Africa and South Asia, indicated by the largest values of α, around 0.23–0.26. The global average yields the smallest α, 0.13.

The second term, $1/\exp(\beta\,CONV)$, is formulated to model the decrease of r_e with CONV (Fig. 4b), especially at large CONV values. This decreasing effect of CONV on r_e is the strongest in South and East Asia, corresponding to the largest β. Figure 4c shows the combination of these two terms, $r_{conv} = [1 - \exp(-CONV/\alpha)]/\exp(\beta\,CONV)$, which captures the initial growth of r_{conv} with CONV, reaching a maximum around CONV=1, and decreasing r_{conv} when CONV further increases. For CONV>1, the decrease of r_{conv} is most noticeable in South and East Asia. Possible causes for the reduction in r_{conv} with increasing CONV include: (1) increased convection distributes more aerosols to the high altitudes in the UT thus affecting ice cloud formation there. For the same columnar AOT, stronger convection may result in increased aerosol effects (reduction of r_e) on ice clouds; (2) the cloud top is higher in stronger convection thus the MODIS r_e is measured at higher altitude with lower cloud top temperature. It is known that ice cloud formed in colder temperature has smaller particle size (e.g. McFarquhar and Heymsfield, 1997).

The third term, $r_{aot} = AOT^{\eta}$, represents the modulation of AOT on r_e (Fig. 4d): increasing aerosol loading increases cloud number density and reduces r_e. The differences among the curves for South America, Southern African and Northern Africa are relatively small, suggesting similar aerosol effects in these three regions. The slope

5 of this term is the largest in South Asia and smallest in East Asia as characterized by the largest and smallest values of $(-\eta)$, respectively. The steep slope for South Asia indicates a strong aerosol influence, while the flatness of the curve for East Asia suggests that increasing aerosols in this region have a relatively small impact on the cloud particle size. On the other hand, the larger value of $(-\eta)$, for the same AOT, $r_{aot} = AOT^{\eta}$

10 yields larger r_e. In this case, r_e is larger for South Asia than East Asia for the same AOT, which may be due to more moisture in the South Asian monsoon region. South America and Africa (Northern and Southern) regions have characteristics in-between those of East and South Asia regions, corresponding to a moderate aerosol effect.

Figure 4e combines the two reduction terms together, $r_{aot}/\exp(\beta CONV) =$

15 $AOT^{\eta}/\exp(\beta CONV)$. South Asia stands out again in Fig. 4e, which shows the strongest reduction rate of r_e with increasing AOT. The combined effects of CONV (r_{conv}) and AOT (r_{aot}) on r_e as computed by the empirical model (Eq. 4) are illustrated by Fig. 4f, which approximately capture the observed relationships (e.g. Fig. 2b, Fig. 3 left column).

6 Conclusions

20 Based on the analysis of 4 years (August 2004 to July 2008) collocated Aura MLS and Aqua MODIS observations, we find that MODIS ice cloud effective radius (r_e) generally increases with convective intensity but decreases with aerosol loading. We use MLS IWC measurement at 215 hPa to indicate convective strength (CONV) and AOT measurement from MODIS to indicate aerosol loading. Using least-squares fitting, we

25 obtain an empirical formula for r_e as a function of CONV and AOT, which approximately captures the observed relationships among r_e, CONV and AOT.

Using this empirical model, we can quantitatively compare the regional differences in the dependence of r_e on CONV and AOT. We find that South Asia and Northern Africa exhibit strong increases of r_e with CONV, while South and East Asia also approach the saturation effect of r_e with CONV quite quickly, possible due to the prevalence of aerosols there. When convection increases, aerosols are lifted high in the atmosphere, causing a reduction of r_e. The South Asia region has the greatest reduction of r_e by unit AOT, with the rate of reduction coefficient is about twice of that in East Asia and 30% higher than the global average. Whether this strong sensitivity of r_e to aerosol amount in South Asia relates to the aerosol composition, the background aerosol concentration, or the dynamical system, warrants further study. It is also worth noting that the empirical fitting converges relatively poorer in South and East Asia than other regions, suggesting the complexity of aerosol-cloud interactions there.

The empirical model represents our first attempt to derive an analytical formula that captures aerosol effects on ice cloud particle size. The approach demonstrates a framework to use satellite data to quantify the first indirect effect of aerosol on ice clouds for use in climate models. With the better height-resolved aerosol and cloud data from CALIPSO and CloudSat, we will continue this work to provide a height-resolved r_e parameterization for simulating the aerosol effect on cloud particle size.

References

Ackerman, A. C., Kirkpatrick, M. P., Stevens, D. E., and Toon, O. B.: The impact of humidity above stratiform clouds on indirect aerosol climate forcing, Nature, 432, 1014–1017, 2004.
Albrecht, B. A.: Aerosols, cloud microphysics, and fractional cloudiness, Science, 245, 1227–1230, 1989.
Evans, K. F. and Stephens, G. L.: Microwave radiative transfer through clouds composed of

Convection and aerosol pollution on ice cloud particle

J. H. Jiang et al.

realistically shaped ice crystals. Part I: Single scattering properties, J. Atmos. Sci., 52, 2041–2057, 1995.

Jiang, J. H., Su, H., Schoeberl, M., Massie, S. T., Colarco, P., Platnick, S., and Livesey, N.: Clean and polluted clouds: relationships among pollution, ice cloud and precipitation in South America, Geophys. Res. Lett., 35, L14804, doi:10.1029/2008GL034631, 2008.

Jiang, J. H., Su, H., Massie, S. T., Colarco, P. R., Schoeberl, M. R., and Platnick, S.: Aerosol-CO relationship and aerosol effect on Ice cloud particle size: Analyses from Aura MLSand Aqua MODIS observations, J. Geophys. Res., 114, D20207, doi:10.1029/2009JD012421, 2009.

Jiang, J. H., Su, H., Pawson, S., Liu, H. C., Read, W., Waters, J. W., Santee, M., Wu, D. L., Schwartz, M., Livesey, N., Lambert, A., Fuller, R., and Lee, J. N.: Five-year (2004–2009) Observations of Upper Tropospheric Water Vapor and Cloud Ice from MLS and Comparisons with GEOS-5 analyses, J. Geophys. Res. 115, D15103, doi:10.1029/2009JD013256, 2010.

Lohmann, U. and Feichter, J.: Global indirect aerosol effects: a review, Atmos. Chem. Phys., 5, 715–737, doi:10.5194/acp-5-715-2005, 2005.

McFarquhar, G. M. and Heymsfield, A. J.: Parameterization of tropical cirrus ice crystal size distributions and implications radiative transfer: Results from CEPEX, J. Atmos. Sci., 54, 2187–2200, 1997.

Matrosov, S. Y., Orr, B. W., Kropfli, R. A., and Snider, J. B.: Retrieval of vertical profiles of cirrus cloud microphysical parameters from Doppler radar and infrared radiometer measurements, J. Appl. Meteor., 33, 617–626, 1994.

Menon, S., Hansen, J., Nazarenko, L., and Luo, Y.: Climate Effects of Black Carbon Aerosols in China and India, Science, 27, 2250–2253, doi:10.1126/science.1075159, 2002.

Mitchell, D. L., Macke, A., and Liu, Y.: Modeling cirrus clouds. Part I: Treatment of bimodal size spectra and case study analysis, J. Atmos. Sci., 53, 2952–2966, 1996.

Penner, J. E., Andreae, M., Annegarn, H., Barrie, L., Feichter, J., Hegg, D., Jayaraman, A., Leaitch, R., Murphy, D., Nganga, J., and Pitari, G.: Chapter 5: Aerosols, their direct and indirect effects, in Climate Change 2001: The Scientific Basis, edited by: Houghton, H. T., Ding, Y., Griggs, D. J., et. al., Report to Intergovernmental Panel on Climate Change from the Scientific Assessment Working Group (WGI), 289–348, Cambridge University Press, 2006.

Platnick, S.: Vertical photon transport in cloud remote sensing problems, J. Geosphys, Res., 105(D18), 22919–22935, 2000.

Platt, C. M. R.: A parameterization of the visible extinction coefficient in terms of the ice/water

content, J. Atmos. Sci., 48, 2083–2098, 1997.

Sherwood, S. C.: Aerosols and ice particle size in tropical cumulonimbus, J. Clim, 15, 1051–1063, 2002.

Su, H., Jiang, J. H., Liu, X., Penner, J. E., Read, W. G., Massie, S. T., Schoeberl, M. R., Colarco, P., Livesey, N. J., and Santee, M. L.: Enhanced Water Vapor Transport to the Stratosphere by Pollutants in Asia, J. Climate, in press, 2010.

Twomey, S.: Atmospheric Aerosols, Elsevier Scientific, Amsterdam, 302 pp., 1977.

Zhang, Z., Platnick, S., Yang, P., Heidinger, A. K., and Comstock, J. M.: Effects of ice particle size vertical inhomogeneity on the passive remote sensing of ice clouds, J. Geophys. Res., 115, D17203, doi:10.1029/2010JD013835, 2010.

Table 1. Values of the empirical fitting parameters in Eq. (4) for various regions. The least-square fits are computed using IWC (mg/m^3) measured by MLS, and r_e (µm) and AOT measured by MODIS from August 2004 to July 2008. The convergence of each fit is indicated by χ^2/DOF.

Region / Fitted Parameter	α	β	η	ε	χ^2/DOF
Global	0.133	0.00543	−0.0661	24.039	0.6
South America	0.183	0.00308	−0.0632	23.795	1.2
Southern Africa	0.201	0.00716	−0.0740	22.684	1.3
Northern Africa	0.259	0.00678	−0.0589	23.703	1.6
South Asia	0.230	0.0258	−0.0838	25.919	3.6
East Asia	0.144	0.0172	−0.0426	24.709	6.9
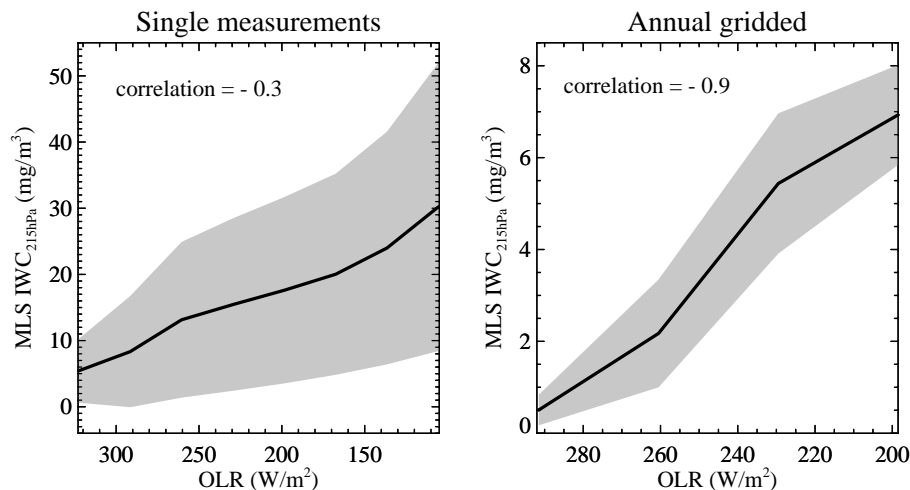
Fig. 1. Left column: the black curve is the MLS measured IWC at 215hPa binned as a function of collocated GEOS-5 OLR. All single MLS IWC measurements between August 2004 and July 2008 in the tropical region (30° S–30° N) are used. The GEOS-5 data are sampled onto the MLS footprints. The standard deviations of the data are indicated by the gray shaded area. Right column: same as left column except for gridded (8° longitude by 4° degree latitude) data averaged for the 4 years.
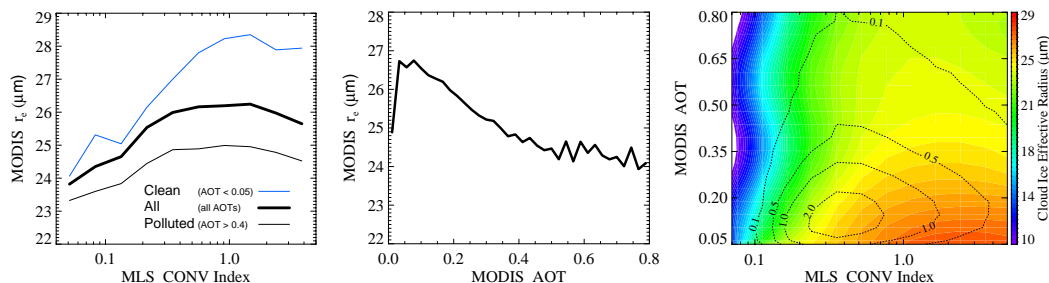
Fig. 2. (a): MODIS measured ice cloud r_e binned according to CONV, based on MLS IWC at 215 hPa. The thick black curve is the average r_e as a function of CONV using all values of AOT. The blue curve is for data with AOT<0.05 and the thin black curve is for data in heavily polluted environment with AOT>0.4. **(b)** MODIS r_e binned according to the MODIS AOT measurements. **(c)** A Bi-Variate Composite (BVC) plot of the r_e-CONV-AOT relation, in which the MODIS r_e data are binned according to both MLS IWC and MODIS AOT. All collocated MODIS and MLS measurements from August 2004 to July 2008 between 50° S to 50° N are used for the plot.
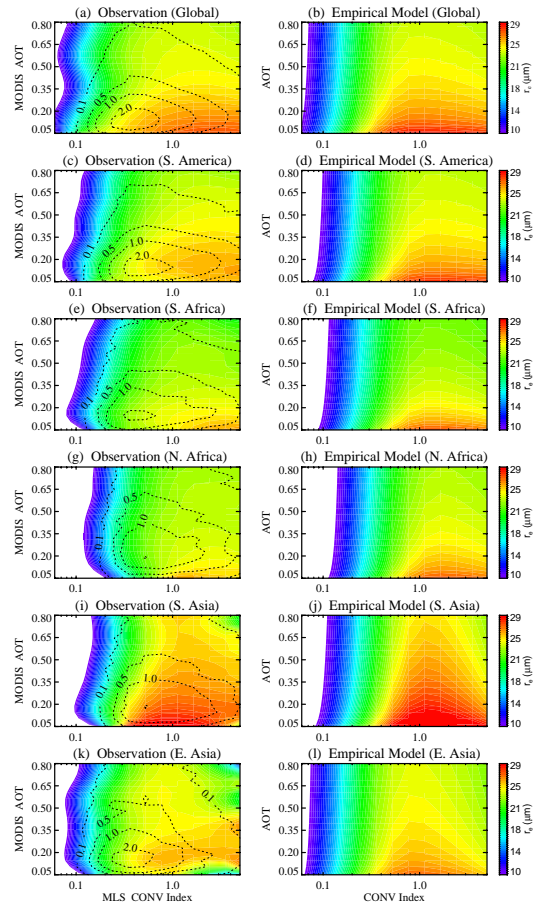
Fig. 3. Left column: observed r_e as a function of CONV and AOT in various regions. Right column: computed r_e as a function of CONV and AOT based on the empirical models for each region.
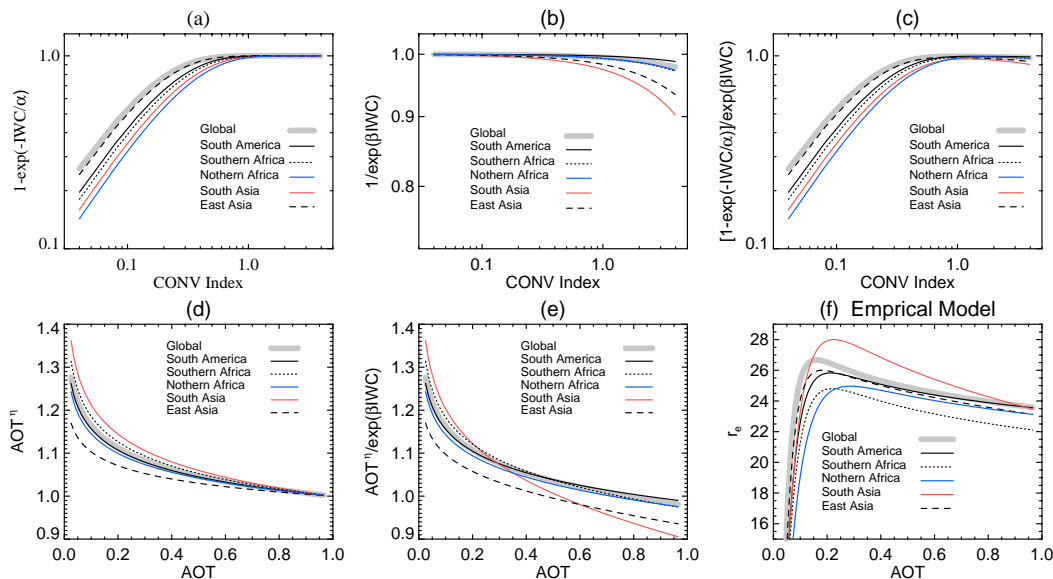
Fig. 4. (a–e) Plots showing how each term (or the combination of two terms) of the empirical models governs r_e in various regions. **(f)** The modeled r_e as a function of AOT for each region.